

Impacts of organic aerosols and its oxidation level on CCN activity from measurement at a suburban site in China

Fang Zhang^{1,2}, Zhanqing Li*^{1,2,3}, Yanan Li^{1,2}, Yele Sun⁴, Zhenzhu Wang⁵, Ping Li^{1,2},

Li Sun⁶, Maureen Cribb³, Chuanfeng Zhao^{1,2}, Qingqing Wang⁴

5 ¹State Key Laboratory of Earth Surface Processes and Resource Ecology, College of Global Change and Earth System Science, Beijing Normal University, Beijing 100875, China

²Joint Center for Global Change Studies, Beijing 100875, China

10 ³Earth System Science Interdisciplinary Center and Department of Atmospheric and Oceanic Science, University of Maryland, College Park, Maryland, USA.

⁴State Key Laboratory of Atmospheric Boundary Layer Physics and Atmospheric Chemistry, Institute of Atmospheric Physics, Chinese Academy of Sciences, Beijing 100029, China

15 ⁵Key Laboratory of Atmospheric Composition and Optical Radiation, Anhui Institute of Optics and Fine Mechanics, Chinese Academy of Sciences, Hefei 230031, China

⁶Liaoning Weather Modification Office, Shenyang, 112000, China

*correspondence to: Z. Li (zli@atmos.umd.edu)

20

Abstract

This study is concerned with the impacts of organic aerosols on CCN activity based on field measurements made at a suburban site in north China. The sensitivity of the estimated CCN number concentration (N_{CCN}) to both volume fraction of organic material (x_{org}) and aerosol oxidation level (using f_{44} , the fraction of m/z 44 in aerosol organic material) are examined. A strong dependence of CCN number concentration (N_{CCN}) on the x_{org} and f_{44} was noted. The sensitivity of volume fraction of organics to N_{CCN} increased with increasing x_{org} . The impacts of the aerosol particles oxidation or aging level on estimating N_{CCN} were also very significant. When the particles were mostly composed of organics ($x_{\text{org}} > 60\%$), the N_{CCN} at the supersaturation of 0.075% and 0.13% was underestimated by 46% and 44% respectively if aerosol particles were freshly emitted with primary organics ($f_{44} < 11\%$); while the underestimation decreased to 32% and 23% at the corresponding supersaturations if the particles were with more hygroscopic secondary organics ($f_{44} > 15\%$). The N_{CCN} at the supersaturation of 0.76% was underestimated by 11% and 4% respectively at $f_{44} < 11\%$ and $f_{44} > 15\%$. But for the particles composed of low organics (e.g. $x_{\text{org}} < 40\%$), the effect caused by the f_{44} was quite insignificant both at high and low supersaturations. This is due to that the overall hygroscopicity of the particles is dominated by inorganics such as sulfate and nitrate, which are more hygroscopic than organic compounds. Our results indicated that it would decrease the uncertainties in estimating N_{CCN} and lead to a more accurate estimation of N_{CCN} to increase the proportion of secondary organics, especially when the composition of the

aerosols is dominated by organics.

The applicability of the CCN activation spectrum obtained at Xinzhou to the Xianghe site, about 400 km to the northeast of Xinzhou, was investigated, with the aim of further examining the sensitivity of N_{CCN} to aerosol type. Overall, the mean
5 CCN efficiency spectrum derived from Xinzhou performs well at Xianghe when the supersaturation levels are $> 0.2\%$ (overestimation of 2-4%). However, N_{CCN} was overestimated by $\sim 20\%$ at supersaturation levels of $< 0.1\%$. This suggests that the overestimation is mainly due to the smaller proportion of aged and oxidized organic aerosols present at Xianghe compared with Xinzhou.

10 **1. Introduction**

11 To reduce the uncertainty of aerosol indirect effects on the radiative balance of
12 the atmosphere, it is important to gain a good knowledge of the ability of aerosol
13 particles to form cloud condensation nuclei (CCN) at the typical supersaturations
14 found in the atmosphere. The CCN activity of aerosol particles is governed by the
15 Köhler theory (Köhler, 1936). This theory determines CCN from aerosol particle size
16 and physicochemical properties, which include the molar volume, activity coefficient,
17 and effect on surface tension (McFiggans et al., 2006). These properties, however, are
18 difficult to measure.

19 Researchers have proposed single-parameter models to parameterize the CCN
20 activation and hygroscopicity of multi-component aerosols (Hudson and Da, 1996;
21 Rissler et al., 2006; Petters and Kreidenweis, 2007; Wex et al., 2007). Field
22 experiments have been conducted with the aim of better characterizing particle
23 physicochemical parameters influencing cloud CCN activation. Due to the large
24 spatial variability of aerosol types and compositions, the CCN activation efficiency
25 varies greatly over different regions. CCN number concentrations (N_{CCN}) can often be
26 better predicted in the background atmosphere (Chuang et al., 2000; Dusek et al.,
27 2003; VanReken et al., 2003; Snider et al., 2003; Rissler et al., 2004; Gasparini et al.,
28 2006; Stroud et al., 2007; Bougiatioti et al., 2009).

29 The largest errors are associated with urban emissions (Sotiropoulou et al., 2007).
30 This is likely due to the organics component of aerosol particles, which have the
31 largest uncertainty and are not fully understood. Biomass burning aerosols and
32 secondary organics formed from the oxidation of common biogenic emissions are
33 often more difficult to activate (Mircea et al., 2005; VanReken et al., 2005; Lee et al.,
34 2006; Varutbangkul et al., 2006; Clarke et al., 2007; Rose et al., 2010; Engelhart et al.,

2012; Paramonov et al., 2013; Lathem et al., 2013; Mei et al., 2013b; Zhang et al., 2014). Particles with aged/oxidized secondary organic components (e.g., organic acids) have been shown to be more hygroscopic (Raymond and Pandis, 2002; Hartz et al., 2006; Bougiatioti et al., 2011), but still much less hygroscopic than inorganic species. The sensitivity of estimated N_{CCN} to organics have been examined in a number of recent studies (Wang et al., 2008; Reutter et al., 2009; Ervens et al., 2010; Kammermann et al., 2010; Ward et al., 2010; Zhang et al., 2012; Mei et al., 2013a). It is widely known that the estimated N_{CCN} is sensitive to changes in organics due to the latter's complex components. The amounts and hygroscopicity parameter of organics (κ_{org}) vary substantially and lead to significant biases in estimating CCN concentrations and aerosol indirect forcing (Sotiropoulou et al., 2007; Hings et al., 2008; Liu and Wang, 2010). Therefore, field investigations regarding CCN activity and organics impacts, especially in heavily polluted regions, are pivotal to better parameterize CCN in climate models.

Northern China is a fast developing and densely populated region of China, where aerosol loading is high (Li et al., 2007, 2011), the particle composition is complex, and severe haze pollution episodes are common (Guo et al., 2014). In recent years, CCN measurements have been collected during field campaigns carried out in the region (Wiedensohler et al., 2009; Gunthe et al., 2011; Yue et al., 2011; Deng et al., 2011, 2013; Zhang et al., 2014). These studies have presented different perspectives on the influence of particle size and composition on CCN activity. For example, Deng et al. (2013) evaluated various schemes for CCN parameterization and recommended that the particle number size distribution (PSD) together with inferred mean size-resolved activation ratios can be used to estimate CCN number concentrations without considering the impact of particle composition. However,

60 Zhang et al. (2014) demonstrated that the 30–40% uncertainties in N_{CCN} are mainly
61 associated with changes in particle composition. None of the above-mentioned studies
62 have investigated the impact of organics on estimating N_{CCN} in Northern China.
63 Zhang et al. (2012) noted a more significant influence of organics on CCN activity but
64 without concerning the influences of particles oxidation or aging on CCN activity; in
65 addition, the campaign average mass fraction of organics in their study was $< 20\%$.

66 The aim of this paper is to examine the sensitivity of CCN activity to aerosol
67 physicochemical properties (especially aerosols containing large amounts of organics,
68 as well as the oxidation level), and also to see how much uncertainty is incurred by
69 applying the CCN efficiency spectra measured at one site to another site in a heavily
70 polluted region. The instrumentation and data used in the study are described in
71 section 2. The method for calculating the hygroscopicity parameter (κ_{chem}) is
72 introduced in section 3. The sensitivity of x_{org} as well as oxidation level of organics on
73 estimating N_{CCN} in section 4, and the ability of the CCN efficiency spectrum observed
74 at the Xinzhou site to represent CCN at the Xianghe site, are also presented and
75 discussed at the last part of this section. Conclusions from the study are given in
76 section 5.

77 2. Measurements and data

78 An intensive observation period field campaign similar to the
79 Aerosol-CCN-Cloud Closure Experiment (Zhang et al., 2014), called the Atmosphere,
80 Aerosol, Cloud, and CCN (A^2C^2) experiment, was conducted from 22 July to 26
81 August of 2014 at Xinzhou ($38.24^\circ N$, $112.43^\circ E$; 1500 m above sea level), a city with a
82 population of 0.51 million in Northern China. The site is located about 360 km
83 southwest of the metropolitan Beijing area and about 10 km south of the local town
84 center. The site is surrounded by agricultural land (e.g., corn) with little local pollution

85 plums from motor vehicles and industrial activities. Sitting between two mountains
86 (Taihang Mountain to the east and Lüliang Mountain to the west), the site also
87 experiences air masses from Xinzhou City to the north and from Taiyuan City to the
88 south, the capital of Shanxi Province. Air masses from the northeast and southwest
89 dominate over the site during summer. Depending on the wind direction,
90 measurements at the Xinzhou site can detect air parcels of urban, rural, or mixed
91 origins, including both fresh biogenic emissions around the site and aged aerosols
92 from advection.

93 **2.1 Instruments and measurements**

94 During the field campaign, a Scanning Mobility Particle Sizer (SMPS),
95 combined with a Droplet Measurement Technologies-Cloud Condensation Nuclei
96 Counter (DMT-CCN_C) (Lance et al., 2006), was used for size-resolved CCN
97 measurements as well as particle number size distribution (PSD) measurements. The
98 measured aerosol PSD is within the size range of 14-600 nm. Aerosol chemical
99 composition was measured simultaneously by an Aerodyne Aerosol Chemical
100 Speciation Monitor (ACSM) (Sun et al., 2012).

101 The aerosol inlet for the size distribution measurements was equipped with a TSI
102 Environmental Sampling System (Model 3031200), which consists of a sharp-cut
103 PM₁ cyclone and a bundled nafion dryer. The size-resolved CCN efficiency spectra
104 were measured by coupling the DMT-CCN_C used with the SMPS (Rose et al., 2008).
105 In this step, the particles are rapidly dried with RH < 30% upon entering the
106 Differential Mobility Analyzer (DMA). Thus, size selection is effectively performed
107 under dry conditions. The nafion dryer and the sheath air inside the DMA are
108 sufficient to remove residual water associated with the ambient particles. Relative

109 deviations in particle diameter should be $< 1\%$. The sample flow exiting the DMA
110 was split into two parts: 0.3 lpm for the CPC and 0.5 lpm for the CCN counter
111 (CCN_C). The DMA, controlled by TSI-AIM software, scanned one size distribution
112 every five minutes. The CCN_C was operated at a total flow rate of 0.5 lpm with a
113 sheath-to-aerosol flow ratio of 10. The inlet RH for CCN_C was $< 30\%$. During the
114 field campaign, the mean sample temperature and pressure measured by CCN_C
115 sensors was $(24.3 \pm 1.4) ^\circ\text{C}$ and (898.4 ± 11.7) hPa. The supersaturations levels of CCN_C
116 were calibrated with ammonium sulfate before and after the field campaign, following
117 the procedures outlined in [Rose et al. \(2008\)](#). During each CCN measurement cycle,
118 calibrated effective supersaturations were set at 0.075%, 0.13%, 0.17%, 0.39%, and
119 0.75%. The overall relative error (1σ) for the supersaturation levels was estimated to
120 be $< 3.5\%$. The completion of a full measurement cycle took 50 minutes (10 minutes
121 for each supersaturation level).

122 The measurement of non-refractory submicron aerosol species including
123 organics, sulfate, nitrate, ammonium, and chloride were made with an ACSM. During
124 the field campaign, ambient aerosols were drawn inside through a $\frac{1}{2}$ inch (outer
125 diameter, the inner diameter is 0.38 inch) stainless steel tube at a flow rate of ~ 3 L
126 min^{-1} , of which ~ 84 cc min^{-1} was sub-sampled into the ACSM. An URG cyclone
127 (Model: URG-2000-30ED) was also positioned in front of the sampling inlet to
128 remove coarse particles with a cut-off size of $2.5 \mu\text{m}$. Before sampling into the ACSM,
129 aerosol particles were dried using a silica gel desiccant. The residence time in the
130 sampling tube was ~ 5 s. The ACSM was operated at a time resolution of ~ 15 min with
131 a scan rate of mass spectrometer at 500 ms amu^{-1} from m/z 10 to 150. Regarding the
132 calibration of the ACSM, mono-dispersed, size-selected 300-nm ammonium nitrate
133 particles within a range of concentrations were sampled into both the ACSM and a

134 condensation particle counter (CPC). The ionization efficiency (IE) was then
135 determined by comparing the response factors of the ACSM to the mass calculated
136 with known particle size and number concentrations from the CPC. More detailed
137 descriptions of the operation and calibration of the ACSM are given in Sun et al.
138 (2012) and Ng et al. (2011). The campaign averaged mass concentration of PM_{10} is
139 $31.6 \mu\text{g m}^{-3}$.

140 In addition to the ACSM, the black carbon (BC) in $PM_{2.5}$ was simultaneously
141 measured at a time resolution of 5 min by a seven-wavelength aethalometer (Model
142 AE31, Magee Scientific Corporation). The campaign averaged mass concentration of
143 BC is $\sim 2.5 \mu\text{g m}^{-3}$. During the experiment, the campaign area was generally hot and
144 dry, with an average temperature of $21.6 \text{ }^\circ\text{C}$ and an average ambient RH of 69.5%.

145 2.2 Data

146 The raw CCN data were first filtered according to instrument recorded
147 parameters (e.g., temperature and flow). For example, if the relative difference
148 between the actual and preset sample flows was larger than 4%, the data are flagged
149 as invalid. The data is also excluded if the “temperature stability” was flagged as “0”.
150 Here, the “temperature stability” refers to the T_1 , T_2 and T_3 in cloud chamber of the
151 CCNc, which is set to obtain the target supersaturations. If the average differences
152 between preset T_1 , T_2 and T_3 and the measured values are larger than $0.4 \text{ }^\circ\text{C}$, the
153 “temperature stability” is flagged as “0”. Thus, the data is invalid and will be removed.
154 A multiple charge correction and transfer function (Deng et al., 2011) is applied to
155 each PSD as well as to the CCN efficiency spectrum. Size-resolved CCN and PSD
156 data, measured with a DMT-CCNc and a SMPS (with a particle size range of 10-700
157 nm) on 7-21 July 2013 at Xianghe (Zhang et al., 2014), are used in this study for

158 comparisons with CCN activity at the Xinzhou site. Aerosol mass concentrations were
159 processed using the ACSM standard data analysis software (version 1.5.3.0). Detailed
160 procedures for the data analysis have been described by Ng et al. (2011) and Sun et al.
161 (2012). The size-resolved CCN activation ratio (size-resolved AR) is defined as the
162 $dN_{CCN}/d\log D_p$ divided by the $dN_{CN}/d\log D_p$. These values were measured by
163 SMPS-DMT-CCNc with particle size selection in the DMA. The bulk activation ratio
164 (bulk AR) is defined as the total CCN concentration divided by the total CN
165 concentration. The total CCN and CN number concentrations are integrated by the
166 measured CCN and CN size distribution respectively over the whole size range.

167 3. Derivation of κ_{chem}

168 In this study, we calculate κ_{chem} based on bulk chemical composition observations
169 made during the field campaign. The method is very similar to that used by Zhang et
170 al., (2014). As proposed by Petters and Kreidenweis (2007), κ_{chem} can be predicted
171 using a simple mixing rule based on chemical volume fractions for a given internal
172 mixture:

$$173 \quad \kappa_{chem} = \sum_i \varepsilon_i \kappa_i \quad (1)$$

174 where κ_i and ε_i are the hygroscopicity parameter and volume fraction, respectively, for
175 the individual (dry) components in the mixture and i is the number of components in
176 the mixture.

177 Measurements from the ACSM in Xinzhou show that the composition of
178 submicron particles was dominated by organics, followed by sulfate, ammonium, and
179 nitrate. The contribution of chloride was negligible (volume fraction of about < 2%).
180 The analysis of the anion and cation balance suggests that anionic species (NO_3^- ,
181 SO_4^{2-}) were essentially neutralized by NH_4^+ over the relevant size range. For
182 refractory species, BC represented a negligible fraction of the total submicron aerosol

183 volume (< 3%). Sea salt and dust are usually coarse mode particles with particle sizes >
184 1 μm (Whitby, 1978). The contribution of such types of aerosols is thus expected to be
185 negligible for sizes < 1 μm . Therefore, the submicron particles measured by the ACSM
186 mainly consisted of organics, $(\text{NH}_4)_2\text{SO}_4$, and NH_4NO_3 . The particle hygroscopicity is
187 thus the volume average of the three participating species:

$$188 \quad \kappa_{chem} = \kappa_{org}\varepsilon_{org} + \kappa_{(\text{NH}_4)_2\text{SO}_4}\varepsilon_{(\text{NH}_4)_2\text{SO}_4} + \kappa_{\text{NH}_4\text{NO}_3}\varepsilon_{\text{NH}_4\text{NO}_3} \quad (2)$$

189 Here, the values of κ for $(\text{NH}_4)_2\text{SO}_4$ and NH_4NO_3 are 0.61 and 0.67, respectively.
190 The following linear function derived by Mei et al. (2013) was used to estimate κ_{org} in
191 this study: $\kappa_{org} = 2.10 \times f_{44} - 0.11$, where f_{44} is the fraction of m/z 44 in total organics.
192 The mean value of κ_{org} during the field campaign is 0.115 ± 0.019 .

193 4. Results and discussion

194 4.1 CCN efficiency spectra

195 During the field campaign at the Xinzhou site, ~790 size-resolved CCN
196 efficiency spectra at five supersaturation levels ranging from 0.075% to 0.76% were
197 measured. Figure 1 shows campaign averaged spectra of the measured CCN
198 efficiency at Xinzhou for supersaturation levels of 0.075%, 0.13%, 0.17%, 0.39%, and
199 0.76%. The observed averaged CCN efficiency spectra during Xianghe campaign in
200 summer 2013 are also shown. Note that the maximum activation fraction (MAF) for
201 Xianghe site showed in Figure 1 is slight lower than that we plotted in Zhang et
202 al.(2014). Because some data points when the MAF value >1 were not processed
203 previously, as resulted in larger mean MAF. But in this paper, the data points with
204 MAF > 1.0 were forced to 1 when $D_p > 300$ nm, which could be completely activated
205 at even lower supersaturations but the MAF would never be larger than 1.0. In Figure
206 1, the right panels show the mass concentration fraction of particle chemical

207 compositions at Xinzhou (top panel) and Xianghe (bottom panel) during their
208 respective observation periods. Significant differences in size-resolved CCN
209 efficiency spectra at the two sites are seen. Aerosol particles at Xinzhou activate more
210 efficiently (higher values of AR) at a given particle diameter (D_p) for the same
211 supersaturation level. In the other words, a larger D_p was required to reach the same
212 activation efficiency at Xianghe. This suggests that aerosol properties at each site
213 differ.

214 The slope of AR with respect to diameters near D_p when AR=50% (defined here
215 as the cut-off diameter, D_{cut}) provides information about the heterogeneity of the
216 composition for size-resolved particles. For an ideal case when all CCN-active
217 particles have the same composition and size, a steep change in AR from 0 to 1 would
218 be observed as D_p reached D_{cut} . A gradual increase in size-resolved AR with D_p
219 suggests that aerosol particles have different hygroscopicities. The steeper slopes of
220 AR around D_{cut} observed at Xinzhou suggest that the particle composition was less
221 heterogeneous with more hygroscopicity than particles at the Xianghe site. This can
222 be partially explained by the magnitudes of the mean κ_{chem} at the two sites (0.42 at
223 Xinzhou and 0.38 at Xianghe). Also, the f_{44} is greater at Xinzhou than at Xianghe. The
224 m/z 44 signal is mostly due to acids (Takegawa et al., 2007; Duplissy et al., 2011) or
225 acid-derived species, such as esters. f_{44} is closely related to the organic oxidation level
226 (Aiken et al., 2008). Oxidized/aged acids are generally more hygroscopic and easily
227 activated. Moreover, the primary inorganic particles at the Xinzhou site are sulfates,
228 with a mass fraction that is two times greater than that measured at Xianghe.
229 Therefore, particles at the Xinzhou site consist of more hygroscopic sulfate-dominant
230 inorganics and aged/oxidized secondary organics and can thus be more efficiently
231 activated at a given D_p , as shown in Fig. 1.

232 4.2 Air mass influences on CCN activity: a case study

233 Because air mass back trajectories combined with ambient air measurements can
234 be used for analyzing large-scale air pollutant transport and source identification at a
235 receptor site (Stohl, 1996; Rousseau et al., 2004), in this study, we calculated five-day
236 (120 hr) back trajectories using the Hybrid Single-Particle Lagrangian Integrated
237 Trajectory (HYSPLIT) model (Draxler and Hess, 1998) with National Centers for
238 Environmental Prediction (NCEP) reanalysis data. TrajStat software (Wang et al.,
239 2009) has been used to calculate trajectories. The arrival height of the trajectories at
240 the Xinzhou site was at the surface.

241 Three cases were selected to study air mass influences on CCN activity: (1) Case
242 1, 19 August 2014, 19:00-21:00 local time (LT); (2) Case 2, 9 August 2014,
243 03:00-10:00 LT; and (3) Case 3, 29 July 2014, 00:00-12:00 LT. Each case is
244 associated with a different CCN efficiency spectrum, i.e., top, middle, and bottom
245 panels of Fig. 2 are for Cases 1, 2, and 3, respectively. Their respective back
246 trajectories are shown in Fig. 3.

247 In Case 1, air trajectories (red line in Fig. 3) originated from the southwest and
248 passed through northern Shaanxi Province and northwestern Shanxi Province, then
249 rounded back to the site from the north/northeast. So, aerosols in this case are closely
250 associated with air parcels north/northeast of the site. The trajectories were very short,
251 suggesting that the air flow was slow during the observational period. Under these
252 circumstances, aerosol loading would be largely impacted by local sources around the
253 site. A high mass fraction of organics ($> 60\%$) with low f_{44} ($\sim 10\%$) and κ_{chem} (< 0.3)
254 values was measured during the observational period. Furthermore, the PSD showed
255 one peak mode with $D_p = 56$ nm and a high N_{CN} ($\sim 1.7 \times 10^4$ cm $^{-3}$), but low mass
256 concentration of PM_{10} (28.36 $\mu\text{g m}^{-3}$). This suggests that particles may be composed of

257 freshly emitted primary aerosols (the biogenic emissions from the plants and trees
258 around the site). This type of aerosol is usually less hygroscopic with a single peak
259 mode primarily composed of fine particles (Whitby, 1978; Hussein et al., 2005).
260 These aerosols cannot activate efficiently. The maximum activation fraction (MAF)
261 shown in the top right panel of Fig. 2 is less than 0.6 at all supersaturation levels for
262 particles with $D_p > 300$ nm, indicating that the particles should be largely externally
263 mixed aerosols.

264 In Case 2 (blue line in Fig. 3), air parcels moved rapidly from the west to the site.
265 The site should then be influenced by the large-scale transport of air masses. For this
266 case, aerosols contain a small amount of organics (< 30%), but have high f_{44} (~14%)
267 and κ_{chem} values (~0.5). The PSD showed a double peak mode with an N_{CN} of
268 $\sim 1.3 \times 10^4$ cm⁻³ and a relatively high mass concentration of PM₁ (81.45 $\mu\text{g m}^{-3}$). The
269 double peak mode suggests that aerosols in this case are a mixture of aerosols from
270 local sources and from other regions (Whitby, 1978; Dal Maso et al., 2007). Because
271 aerosols are aged and oxidized during long-distance transport, these particles are
272 usually composed of secondary organic and inorganic components with more
273 hygroscopicity (Weber et al., 1999; Verver et al., 2000). These aerosols can activate
274 efficiently. The MAF is close to 1 and the slopes of AR around D_{cut} are steep at all
275 supersaturation levels (middle right panel of Fig. 2). This CCN efficiency spectrum is
276 similar to the ideal spectrum of pure ammonium sulfate.

277 In Case 3 (green line in Fig. 3), air parcels travelled from the northwest to the
278 site. Air masses arriving at the site in this case had passed over densely populated
279 regions with more heavy pollution. A gradual increase in size-resolved AR with D_p is
280 seen (bottom right panel of Fig. 2). This is attributed to the diversity in aerosol
281 hygroscopicity because of the complex nature of the chemical composition of aerosol

282 particles.

283 **4.3 Correlation of N_{CN} and N_{CCN}**

284 Figure 4 shows N_{CN} as a function of N_{CCN} for different supersaturation levels at
285 the Xinzhou and Xianghe sites. They showed high or moderate correlations at high
286 supersaturation levels (e.g., $R^2 = 0.57$ at Xinzhou and $R^2 = 0.85$ at Xianghe at a
287 supersaturation level of $\sim 0.8\%$), but quite poor correlations at low supersaturation
288 levels. Although [Andreae \(2009\)](#) proposed using the relationship of CCN and CN, or
289 even aerosol optical depth (AOD), to parameterize CCN in models, it would lead to
290 large uncertainties especially when the supersaturations are low. It was noticed that
291 there was an apparent higher degree of correlation at Xianghe site for each
292 supersaturation than that derived at Xinzhou site. In view of the similar regimes from
293 which the data are taken and the same instruments by which they have been collected, the
294 discrepancy between Xianghe and Xinzhou should be caused largely by the spatial variations
295 of aerosols types. These variations are primarily attributed to variations in aerosol
296 particle size, i.e., the shape of the PSD as well as particle composition. As presented
297 by [Zhang et al. \(2014\)](#), the relationship between bulk activation ratios and N_{CN} was
298 complex under polluted conditions and was heavily dependent on the
299 physicochemical properties of atmospheric aerosols.

300 **4.4 Impact of x_{org} on N_{CCN}**

301 Precise quantification of N_{CCN} is crucial for understanding aerosol indirect
302 effects and characterizing these effects in models. A CCN closure study is useful to
303 examine the controlling physical and chemical factors and to help verify experimental
304 results. N_{CCN} is usually derived from measured aerosol properties, such as PSD and
305 composition or hygroscopicity based on the Köhler theory. Achieving such closure

306 under heavily polluted conditions is more challenging, especially due to the complex
307 effects of organics on CCN activity. In this section, we examine the sensitivity of
308 N_{CCN} to both volume fraction of organics (x_{org}) and oxidation or aging of organics
309 based on measurement at Xinzhou site. During the observed period, aerosols at the
310 Xinzhou site were dominated by organics, with 12%, 23%, 39%, and 25% of the data points
311 corresponding to $x_{org} > 60\%$, $50\% < x_{org} < 60\%$, $40\% < x_{org} < 50\%$ and $x_{org} < 40\%$, respectively.
312 For the purpose of examining the sensitivity of estimated N_{CCN} to x_{org} and
313 oxidation/aging level, we sorted the size-resolved CCN data when the $x_{org} > 60\%$,
314 $50\% < x_{org} < 60\%$, $40\% < x_{org} < 50\%$ and $x_{org} < 40\%$. Furthermore, for each level of x_{org} , we
315 tested the impacts on N_{CCN} estimation both from the most oxidized (with f_{44} of higher
316 than 15%) and least oxidized (those primary organic aerosols with f_{44} of lower than
317 11%) organic particles. For example, the size-resolved CCN data points during the
318 period when $x_{org} > 60\%$ and also $f_{44} > 15\%$ was averaged to generate the averaged CCN
319 efficiency spectra at the five supersaturations respectively. Then we used the produced
320 averaged CCN efficiency spectra to estimate N_{CCN} .

321 Estimated CCN size distributions at the five supersaturations were firstly
322 calculated by multiplying the averaged CCN efficiency spectrum (by using the
323 averaged CCN efficiency spectra, the aerosol particles were assumed with uniform
324 chemical composition without considering the effects of the temporal variations of the
325 activation curves on CCN activity) with the actually measured PSD. Then, we
326 integrated the estimated CCN size distribution over the whole size range to generate
327 estimated N_{CCN} . While the measured CCN size distributions are integrated to produce
328 the observed N_{CCN} .

329 Observed and estimated N_{CCN} at four supersaturation levels (0.075%, 0.13, 0.17
330 and 0.76%) were showed in Fig 5. The data points presented more disperse and

331 weaker correlations at lower supersaturations. The sensitivity of volume fraction of
332 organics to N_{CCN} increased with increasing x_{org} . This is especially for the case of these
333 primary organic particles with $f_{44}<11\%$: the slopes obtained from a linear fit of
334 estimated and measured N_{CCN} in Fig 6 decreased rapidly (almost with a decrease of
335 $\sim 50\%$) when the x_{org} varied from $<40\%$ to $>60\%$ at supersaturations of 0.075% , while
336 it didn't exhibit a lot of reduction (merely $\sim 10\%$) along with the increasing of x_{org} for
337 the supersaturation of 0.76% . N_{CCN} was estimated most accurately at higher
338 supersaturation levels. This is likely because a large fraction of particles was already
339 CCN-active. Also, particle composition has relatively less influence on CCN
340 activation at high supersaturations (Twohy and Anderson, 2008). For the oxidized or
341 aged particles with $f_{44}>15\%$, the slopes still follow the similar tendency with the
342 variations of x_{org} at low and high supersaturations but changed more smoothly to the
343 x_{org} attributing to the oxidized/aged organic particles being more hygroscopic.

344 However, the impacts of the aerosol particles oxidization level on estimating
345 N_{CCN} were also very significant. For example, when the particles were composed by
346 large amounts of organics ($x_{org}>60\%$), the N_{CCN} at the supersaturation of 0.075% and
347 0.13% was underestimated by 46% and 44% respectively at $f_{44}<11\%$, while the
348 underestimation decreased to 32% and 23% at the corresponding supersaturation level
349 at $f_{44}>15\%$. The N_{CCN} at $ss=0.76$ was underestimated by 11% and 4% respectively at
350 $f_{44}<11\%$ and $f_{44}>15\%$. One thus could conclude that the estimation of N_{CCN} would be
351 largely improved if the aerosol particles were aged with high oxidation level,
352 especially when the chemical composition of the particles is dominated by organics.
353 But for the particles with relative low organics ($x_{org}<40\%$), the effect caused by the f_{44}
354 was quite insignificant both for high and low supersaturations. In Fig 6, the slopes
355 were all around 1.0 at the two cases of $f_{44}<11\%$ and $f_{44}>15\%$. This can be easily

356 explained. When x_{org} is less than 40%, the overall hygroscopicity of the particles is
357 dominated by inorganic species such as sulfate and nitrate, which are more
358 hygroscopic (κ_{inorg} usually larger than 0.6) than organic compounds (κ_{org} usually
359 smaller than 0.2). As a result, a larger fraction of particles can be activated. According
360 to the simple mixing rule based on chemical volume fractions proposed by [Petters and](#)
361 [Kreidenweis \(2007\)](#), the contribution from organics is quite small. If x_{org} is greater
362 than 60%, organics will dominate the overall particle hygroscopicity. Particles with a
363 large f_{44} are much more hygroscopic and thus strongly influence the estimated N_{CCN} .
364 Our results indicated that increasing the proportion of secondary organics would
365 decrease the uncertainties in estimating N_{CCN} and lead to a more accurate estimation
366 of N_{CCN} .

367 **4.5 Applicability of CCN efficiency spectra**

368 As a means of testing the applicability of the CCN activation spectra, campaign
369 mean CCN efficiency spectra at different supersaturations observed at the Xinzhou
370 site is used to estimate N_{CCN} at the Xinzhou and Xianghe sites respectively, which
371 helps to further examine the sensitivity of N_{CCN} to aerosol type. Data from the two
372 sites were measured during the warm season so that the effect of temporal variations
373 in aerosols on CCN levels is reduced. Fitted campaign mean CCN efficiency spectrum
374 at the five supersaturations at Xinzhou (corresponding to spectra in Fig. 1) is
375 multiplied by dry PSDs actually measured at Xinzhou and at the Xianghe site
376 respectively. This generates estimated CCN size distributions at the two sites. They
377 are then integrated over the whole size range (14-600 nm and 10-700 nm at the
378 Xinzhou and Xianghe sites, respectively) to obtain the estimated N_{CCN} . The measured
379 CCN size distributions at each site are integrated to produce the observed N_{CCN} .

380 Figure 7 shows estimated N_{CCN} as a function of measured N_{CCN} for different
381 supersaturation levels at the two sites. N_{CCN} at Xinzhou was underestimated by 4-5%
382 at supersaturation levels of 0.39% and 0.76%, and was slightly overestimated (~2%)
383 at Xianghe for the same supersaturation levels. Good agreement is seen at the 0.39%
384 and 0.76% supersaturation levels for data from both sites ($R^2 > 0.92$). N_{CCN} at
385 Xinzhou was underestimated by ~7% at supersaturation levels $< 0.1\%$ ($R^2 = 0.87$). At
386 Xianghe, however, N_{CCN} was overestimated by 19-23% at supersaturation levels $< 0.1\%$
387 although the correlation between calculated and measured N_{CCN} was good. Because
388 size-resolved CCN efficiency spectra were applied here, excluding the impact of
389 particle size, the influence of chemical composition on CCN activation can be
390 investigated. The poor estimates of CCN at low supersaturation levels could be
391 attributed to the high sensitivity of N_{CCN} to chemical composition. Because the mass
392 fractions of inorganics and organics measured at the two sites are similar (Fig. 1) and
393 the hygroscopicity for inorganic components is fixed, this overestimation is attributed
394 to the smaller proportion of aged and oxidized organic aerosols at Xianghe compared
395 with aerosols at Xinzhou ($f_{44} = 17\%$ and 11% at Xinzhou and Xianghe, respectively).

396 5. Summary and conclusions

397 In this study, we have investigated the impacts of particle physicochemical
398 properties on CCN activity based on field measurements obtained from 22 July to 26
399 August of 2014 in the suburb of Xinzhou, China. Five-day back trajectories combined
400 with measurements were analyzed to examine air mass influences on CCN activity.
401 CCN efficiency was largely reduced by local air masses, and the MAF was low to
402 $< 60\%$, suggesting externally-mixed and the heterogeneity of particle composition for
403 local emitted aerosols. The CCN activation efficiency was enhanced significantly
404 when the site was under the influence of air transported from far away, during which

405 aerosols could be mixed well with more hygroscopic secondary organic and inorganic
406 components. The relationship between N_{CN} and N_{CCN} was generally poor. Large
407 errors would arise if using the former to estimate the latter, especially under low
408 supersaturation conditions.

409 The sensitivity of N_{CCN} estimation to both x_{org} and f_{44} has also been examined. A
410 strong dependence of N_{CCN} on the both two parameters was noted. The sensitivity of
411 N_{CCN} to volume fraction and particles oxidization or aging level of organics increased
412 with increase of x_{org} . And also this dependence weakens as the supersaturation level
413 increases. When the particles were mostly composed of organics ($x_{org}>60\%$), the N_{CCN}
414 at the supersaturation of 0.075% and 0.13% was underestimated by 46% and 44%
415 respectively if aerosol particles were freshly emitted with primary organics ($f_{44}<11\%$);
416 while the underestimation decreased to 32% and 23% at the corresponding
417 supersaturations if the particles were with more hygroscopic secondary
418 organics($f_{44}>15\%$). The N_{CCN} at the supersaturation of 0.76% was underestimated by
419 11% and 4% respectively at $f_{44}<11\%$ and $f_{44}>15\%$. But for the particles composed of
420 low organics (e.g. $x_{org}<40\%$), the effect caused by the f_{44} was quite insignificant both
421 at high and low supersaturations. This is due to that the overall hygroscopicity of the
422 particles is dominated by inorganics such as sulfate and nitrate, which are more
423 hygroscopic than organic compounds. Our results indicated that it would lead to a
424 more accurate estimation of N_{CCN} to increase the proportion of secondary organics,
425 especially when the composition of the aerosols is dominated by organics.

426 The applicability of the CCN efficiency spectrum measured at the Xinzhou site
427 to the Xianghe site was examined and a good agreement was found when the
428 supersaturation level was $> 0.2\%$. However, N_{CCN} at the Xianghe site was
429 overestimated by 19-23% when the supersaturation level was $< 0.1\%$. Because of the

430 similar mass fractions of inorganics and organics measured at the two sites, we
431 conclude that this overestimation was mainly caused by the smaller proportion of
432 aged and oxidized organic aerosols at Xianghe compared with aerosols at Xinzhou.

433 **Acknowledgements**

434 This work was funded by the National Basic Research Program of China ‘973’ (Grant
435 No. 2013CB955801, 2013CB955804), the Fundamental Research Funds for the
436 Central Universities (Grant No. 2013YB35) and the NSCF-TAMU Collaborative
437 Research Grant Program (Grant No. 4141101031). We also acknowledge the members
438 of the A²C² team for their hard work during the campaign, including Mr. Du Wei
439 (from the State Key Laboratory of Atmospheric Boundary Layer Physics and
440 Atmospheric Chemistry of the Institute of Atmospheric Physics/Chinese Academy of
441 Sciences for carrying out the chemical composition measurements) and Mr. Yuan
442 Cheng (from Nanjing University who helped make the size-resolved CCNc
443 measurements).

444 **References**

445 Aiken, A. C., DeCarlo, P. F., Kroll, J. H., Worsnop, D. R., Huffman, J. A., Docherty,
446 K. S., Ulbrich, I. M., Mohr, C., Kimmel, J. R., Sueper, D., Sun, Y., Zhang, Q.,
447 Trimborn, A., Northway, M., Ziemann, P. J., Canagaratna, M. R., Onasch, T. B.,
448 Alfarra, M. R., Prevot, A. S. H., Dommen, J., Duplissy, J., Metzger, A.,
449 Baltensperger, U., and Jimenez, J. L.: O/C and OM/OC ratios of primary,
450 secondary, and ambient organic aerosols with high-resolution time-of-flight aerosol
451 mass spectrometry, *Environ. Sci. Technol.*, 42, 4478–4485, 2008.

452 Andreae, M.O.: Correlation between cloud condensation nuclei concentration and
453 aerosol optical thickness in remote and polluted regions, *Atmos. Chem. Phys.*, 9,

- 454 543-556, 2009.
- 455 Bougiatioti, A., Fountoukis, C., Kalivitis, N., Pandis, S. N., Nenes, A., and
456 Mihalopoulos, N.: Cloud condensation nuclei measurements in the marine
457 boundary layer of the eastern Mediterranean: CCN closure and droplet growth
458 kinetics. *Atmos. Chem. Phys.*, 9, 7053–7066, 2009.
- 459 Bougiatioti, A., Nenes, A., Fountoukis, C., Kalivitis, N., Pandis, S. N., and
460 Mihalopoulos, N.: Size-resolved CCN distributions and activation kinetics of aged
461 continental and marine aerosol, *Atmos. Chem. Phys.*, 11, 8791-8808,
462 doi:10.5194/acp-11-8791-2011, 2011.
- 463 Chuang, P. Y., Collins, D. R., Pawlowska, H., Snider, J. R., Jonsson, H. H., Brenguier,
464 J. L., Flagan, R. C., and Seinfeld, J. H.: CCN measurements during ACE-2 and
465 their relationship to cloud microphysical properties, *Tellus B*, 52, 843–867, 2000.
- 466 Clarke, A., McNaughton, C., Kasputin, V. N., Shinozuka, Y., Howell, S., Dibb, J.,
467 Zhou, J., Anderson, B., Brekhovskikh, V., Turner, H., and Pinkerton, M.: Biomass
468 burning and pollution aerosol over North America: Organic components and their
469 influence on spectral optical properties and humidification response, *J. Geophys.*
470 *Res.*, 112, D12S18, doi:10.1029/2006JD007777, 2007.
- 471 Dal Maso, M., L. Sogacheva, P. P. Aalto, I. Riipinen, M. Komppula, P. Tunved, L.
472 Korhonen, V. SUUR@USKI, A. Hirsikko, and T. KurtEN, Aerosol size
473 distribution measurements at four Nordic field stations: identification, analysis
474 and trajectory analysis of new particle formation bursts, *Tellus B*, 2007, 59(3),
475 350-361.
- 476 Deng, Z., Zhao, C., Ma, N., Liu, F., Ran, L., Xu, W., Liang, Z., Liang, S., Huang, M.,
477 Ma, X., Zhang, Q., Quan, J., and Yan, P.: Size- resolved and bulk activation
478 properties of aerosols in the North China Plain. *Atmos. Chem. Phys.*, 11,

- 479 3835-3846, 2011.
- 480 Deng, Z., Zhao, C., Ma, N., Ran, L., Zhou, G., Lu, D., and Zhou, X.: An examination
481 of parameterizations for the CCN number concentration based on in situ
482 measurements of aerosol activation properties in the North China Plain, *Atmos.*
483 *Chem. Phys.*, 13, 6227–6237, doi:10.5194/acp-13-6227-2013, 2013.
- 484 Draxler, R., R. and Hess, G., D. 1998. An overview of the HYSPLIT 4 modeling
485 system for trajectories, dispersion, and deposition, *Aust. Meteorol. Mag.* 47, 295–
486 308.
- 487 Duplissy, J., DeCarlo, P. F., Dommen, J., Alfarra, M. R., Metzger, A., Barmpadimos,
488 I., Prevot, A. S. H., Weingartner, E., Tritscher, T., Gysel, M., Aiken, A. C., Jimenez,
489 J. L., Canagaratna, M. R., Worsnop, D. R., Collins, D. R., Tomlinson, J., and
490 Baltensperger, U.: Relating hygroscopicity and composition of organic aerosol
491 particulate matter, *Atmos. Chem. Phys.*, 11, 1155–1165,
492 doi:10.5194/acp-11-1155-2011, 2011.
- 493 Dusek, U., Covert, D. S., Wiedensohler, A., Neususs, C., Weise, D., and Cantrell, W.:
494 Cloud condensation nuclei spectra derived from size distributions and hygroscopic
495 properties of the aerosol in coastal south-west Portugal during ACE-2, *Tellus B*, 55,
496 35–53, 2003.
- 497 Engelhart, G. J., Hennigan, C. J., Miracolo, M. A., Robinson, A. L., and Pandis, S. N.:
498 Cloud condensation nuclei activity of fresh primary and aged biomass burning
499 aerosol, *Atmos. Chem. Phys.*, 12, 7285–7293, doi:10.5194/acp-12-7285-2012,
500 2012.
- 501 Ervens, B., Cubison, M. J., Andrews, E., Feingold, G., Ogren, J.A., Jimenez, J. L.,
502 Quinn, P. K., Bates, T. S., Wang, J., Zhang, Q., Coe, H., Flynn, M., and Allan, J. D.:
503 CCN predictions using simplified assumptions of organic aerosol composition and

- 504 mixing state: a synthesis from six different locations, *Atmos. Chem. Phys.*, 10,
505 4795–4807, doi:10.5194/acp-10-4795-2010, 2010.
- 506 Gasparini, R., Collins, D. R., Andrews, E., Sheridan, P. J., Ogren, J. A., and Hudson, J.
507 G.: Coupling aerosol size distributions and size-resolved hygroscopicity to predict
508 humidity-dependent optical properties and cloud condensation nuclei spectra., *J.*
509 *Geophys. Res.*, 111, D05S13, doi:10.1029/2005JD006092, 2006.
- 510 Gunthe SS; Rose D; Su H; Garland RM; Achtert P; Nowak A; Wiedensohler A;
511 Kuwata M; Takegawa N; Kondo Y; Hu M; Shao M; Zhu T; Andreae MO; Pöschl
512 U (2011) Cloud condensation nuclei (CCN) from fresh and aged air pollution in
513 the megacity region of Beijing, *Atmospheric Chemistry and Physics*, 11,
514 pp.11023-11039. doi: 10.5194/acp-11-11023-2011
- 515 Guo, S., Hu, M., Zamora, M. L., Peng, J., Shang, D., Zheng, J., Zhuofei Du, Zhijun
516 Wu, Min Shao, Limin Zeng, Mario J. Molina,¹ and Zhang, R. (2014).
517 Elucidating severe urban haze formation in China. *Proceedings of the National*
518 *Academy of Sciences of the United States of America*, 111(49), 17373–17378.
519 doi:10.1073/pnas.1419604111
- 520 Hartz, K. E. H., Tischuk, J. E., Chan, M. N., Chan, C. K., Donahue, N. M., and Pandis,
521 S. N.: Cloud condensation nuclei activation of limited solubility organic aerosol,
522 *Atmos. Environ.*, 40, 605–617, 2006.
- 523 Hings, S. S., Wrobel, W. C., Cross, E. S., Worsnop, D. R., Davidovits, P., and Onasch,
524 T. B.: CCN activation experiments with adipic acid: effect of particle phase and
525 adipic acid coatings on soluble and insoluble particles, *Atmos. Chem. Phys.*, 8,
526 3735–3748, doi:10.5194/acp-8-3735-2008, 2008.
- 527 Hudson, J. G. and Da, X. Y.: Volatility and size of cloud condensation nuclei, *J.*
528 *Geophys. Res.*, 101, 4435–4442, 1996.

- 529 Hussein, T., M. Dal Maso, T. PETÄJÄ, I. K. KOPONEN, P. PAATERO, P. P.
530 AALTO, K. HÄMERI, and M. KULMALA, Evaluation of an automatic
531 algorithm for fitting the particle number size distributions, *BOREAL*
532 *ENVIRONMENT RESEARCH*, 2005, 10(5), 337-355.
- 533 Junge, C. and McLaren, E.: Relationship of cloud nuclei spectra to aerosol size
534 distribution and composition, *J. Atmos. Sci.*, 28, 382–390, 1971.
- 535 Kammermann, L., Gysel, M., Weingartner, E., Herich, H., Cziczo, D. J., Holst, T.,
536 Svenningsson, B., Arneth, A., and Baltensperger, U.: Subarctic atmospheric aerosol
537 composition: 3. Measured and modeled properties of cloud condensation nuclei, *J.*
538 *Geophys. Res.*, 115, D04202, doi:10.1029/2009JD012447, 2010.
- 539 Köhler, H.: The nucleus in and growth of hygroscopic droplets, *Trans. Faraday Soc.*,
540 32, 1152–1161, doi:10.1039/TF9363201152, 1936.
- 541 Lance, S., Medina, J., Smith, J., and Nenes, A.: Mapping the operation of the DMT
542 continuous flow CCN counter, *Aerosol Sci. Technol.*, 40, 242–254, 2006.
- 543 Latham, T. L., Beyersdorf, A. J., Thornhill, K. L., Winstead, E. L., Cubison, M. J.,
544 Hecobian, A., Jimenez, J. L., Weber, R. J., Anderson, B. E., and Nenes, A.: Analysis
545 of CCN activity of Arctic aerosol and Canadian biomass burning during summer
546 2008, *Atmos. Chem. Phys.*, 13, 2735-2756, doi:10.5194/acp-13-2735-2013, 2013.
- 547 Lee, Y. S., Collins, D. R., Li, R. J., Bowman, K. P., and Feingold, G.: Expected
548 impact of an aged biomass burning aerosol on cloud condensation nuclei and cloud
549 droplet concentrations, *J. Geophys. Res.*, 111, D22204, doi:10.1029/2005JD006464,
550 2006.
- 551 Li, Z., Chen, H., Cribb, M., Dickerson, R. E., Holben, B., Li, C., Lu, D., Luo, Y.,
552 Maring, H., Shi, G., Tsay, S.-C., Wang, P., Wang, Y., Xia, X., Zheng, Y., Yuan, T.,
553 and Zhao, F.: Preface to special section on East Asian Studies of Tropospheric

- 554 Aerosols: An International Regional Experiment (EASTAIRE), *J. Geophys. Res.*,
 555 112, D22S00, doi:10.1029/2007JD008853, 2007.
- 556 Li, Z., Li, C., Chen, H., Tsay, S.-C., Holben, B., Huang, J., Li, B., Maring, H., Qian,
 557 Y., Shi, G., Xia, X., Yin, Y., Zheng, Y., and Zhuang, G.: East Asian Studies of
 558 Tropospheric Aerosols and Impact on Regional Climate (EAST - AIRC): An
 559 overview, *J. Geophys. Res.*, 116, D00K34, doi:10.1029/2010JD015257, 2011.
- 560 Liu, X. and Wang, J.: How important is organic aerosol hygroscopicity to aerosol
 561 indirect forcing? *Environ. Res. Lett.*, 5, 044010,
 562 doi:10.1088/1748-9326/5/4/044010, 2010.
- 563 McFiggans, G., Artaxo, P., Baltensperger, U., Coe, H., Facchini, M. C., Feingold, G.,
 564 Fuzzi, S., Gysel, M., Laaksonen, A., Lohmann, U., Mentel, T. F., Murphy, D. M.,
 565 O'Dowd, C. D., Snider, J. R., and Weingartner, E.: The effect of physical and
 566 chemical aerosol properties on warm cloud droplet activation, *Atmos. Chem. Phys.*,
 567 6, 2593–2649, doi:10.5194/acp-6-2593-2006, 2006.
- 568 Mei, F., Hayes, P. L., Ortega, A. M., Taylor, J. W., Allan, J. D., Gilman, J. B., Kuster,
 569 W. C., de Gouw, J. A., Jimenez, J. L., and Wang, J.: Droplet activation properties
 570 of organic aerosols observed at an urban site during CalNex-LA, *J. Geophys. Res.*,
 571 118(7), 2903-2917, doi: 10.1002/jgrd.50285, 2013b.
- 572 Mei, F., Setyan, A., Zhang, Q., and Wang, J.: CCN activity of organic aerosols
 573 observed downwind of urban emissions during CARES, *Atmos. Chem. Phys.*, 13,
 574 12155–12169, doi:10.5194/acp-13-12155-2013, 2013a.
- 575 Mircea, M., Facchini, M. C., Decesari, S., Cavalli, F., Emblico, L., Fuzzi, S., Vestin,
 576 A., Rissler, J., Swietlicki, E., Frank, G., Andreae, M. O., Maenhaut, W., Rudich, Y.,
 577 and Artaxo, P.: Importance of the organic aerosol fraction for modeling aerosol
 578 hygroscopic growth and activation: a case study in the Amazon Basin, *Atmos.*

- 579 Chem. Phys., 5, 3111–3126, 2005, <http://www.atmos-chem-phys.net/5/3111/2005/>.
- 580 Ng, N. L., Herndon, S. C., Trimborn, A., Canagaratna, M. R., Croteau, P. L., Onasch,
581 T. B., Sueper, D., Worsnop, D. R., Zhang, Q., Sun, Y. L., and Jayne, J. T.: An
582 Aerosol Chemical Speciation Monitor (ACSM) for Routine Monitoring of the
583 Composition and Mass Concentrations of Ambient Aerosol, *Aerosol Sci. Tech.*, 45,
584 770–784, 2011.
- 585 Paramonov, M., Aalto, P. P., Asmi, A., Prisle, N., Kerminen, V.-M., Kulmala, M., and
586 Petäjä T.: The analysis of size-segregated cloud condensation nuclei counter
587 (CCNC) data and its implications for aerosol-cloud interactions, *Atmos. Chem.*
588 *Phys. Discuss.*, 13, 9681-9731, doi:10.5194/acpd-13-9681-2013, 2013.
- 589 Petters, M. D., and Kreidenweis, S. M.: A single parameter representation of
590 hygroscopic growth and cloud condensation nucleus activity, *Atmos. Chem. Phys.*,
591 7, 1961–1971, doi:10.5194/acp-7-1961-2007, 2007.
- 592 Petters, M. D. and Kreidenweis, S. M.: A single parameter representation of
593 hygroscopic growth and cloud condensation nucleus activity – Part 2: Including
594 solubility, *Atmos. Chem. Phys.*, 8, 6273–6279, doi:10.5194/acp-8-6273-2008,
595 2008.
- 596 Raymond, T. M., and Pandis, S. N.: Cloud activation of single component organic
597 aerosol particles, *J. Geophys. Res.*, 107, 4787, doi:10.1029/2002JD002159, 2002.
- 598 Reutter, P., Su, H., Trentmann, J., Simmel, M., Rose, D., Gunthe, S. S., Wernli, H.,
599 Andreae, M. O., and Pöschl, U.: Aerosol- and updraft-limited regimes of cloud
600 droplet formation: influence of particle number, size and hygroscopicity on the
601 activation of cloud condensation nuclei (CCN), *Atmos. Chem. Phys.*, 9, 7067–7080,
602 doi:10.5194/acp-9-7067-2009, 2009.
- 603 Rissler, J., Swietlicki, E., Zhou, J., Roberts, G., Andreae, M. O., Gatti, L. V., and

- 604 Artaxo, P.: Physical properties of the submicrometer aerosol over the Amazon rain
605 forest during the wet to dry season transition – comparison of modeled and
606 measured CCN concentrations, *Atmos. Chem. Phys.*, 4, 2119–2143,
607 <http://www.atmos-chem-phys.net/4/2119/2004/>, 2004.
- 608 Rissler, J., Vestin, A., Swietlicki, E., Fisch, G., Zhou, J., Artaxo, P., and Andreae, M.
609 O.: Size distribution and hygroscopic properties of aerosol particles from
610 dry-season biomass burning in Amazonia, *Atmos. Chem. Phys.*, 6, 471–491,
611 doi:10.5194/acp-6-471-2006, 2006.
- 612 Rose, D., Gunthe, S. S., Mikhailov, E., Frank, G. P., Dusek, U., Andreae, M. O., and
613 Poschl, U.: Calibration and measurement uncertainties of a continuous-flow cloud
614 condensation nuclei counter (DMT-CCNC): CCN activation of ammonium sulfate
615 and sodium chloride aerosol particles in theory and experiment, *Atmos. Chem.*
616 *Phys.*, 8, 1153–1179, 2008, <http://www.atmos-chem-phys.net/8/1153/2008/>.
- 617 Rose, D., Nowak, A., Achtert, P., Wiedensohler, A., Hu, M., Shao, M., Zhang, Y.,
618 Andreae, M. O., and Poschl, U.: Cloud condensation nuclei in polluted air and
619 biomass burning smoke near the mega-city Guangzhou, China – Part 1:
620 Size-resolved measurements and implications for the modeling of aerosol particle
621 hygroscopicity and CCN activity, *Atmos. Chem. Phys.*, 10, 3365–3383,
622 doi:10.5194/acp-10-3365-2010, 2010.
- 623 Rousseau, D., D., Duzer, D., Etienne, J., L., Cambon, G., Jolly, D. And coauthors.
624 2004. Pollen record of rapidly changing air trajectories to the North Pole, *J.*
625 *Geophys. Res.* 109, D06116, doi:10.1029/2003JD003985.
- 626 Snider, J.R., Guibert, S., Brenguierand, J. L. and Putaud, J. P.: Aerosol activation in
627 marine stratocumulus clouds: Part – II Köhler and parcel theory closure studies, *J.*
628 *Geophys. Res.*, 108, doi:10.1029/2002JD002692, 2003

- 629 Sotiropoulou, R. E. P., Nenes, A., Adams, P. J., and Seinfeld, J. H.: Cloud
630 condensation nuclei prediction error from application of Köhler theory:
631 Importance for the aerosol indirect effect, *J. Geophys. Res.*, 112, D12202,
632 doi:10.1029/2006JD007834, 2007.
- 633 Stohl, A. 1996, Trajectory statistics - a new method to establish source-receptor
634 relationships of air pollutants and its application to the transport of particulate
635 sulfate in Europe, *Atmos. Environ.* 30, 579–587.
- 636 Stroud, C. A., Nenes, A., Jimenez, J. L., DeCarlo, P., Huffman, J. A., Bruintjes, R.,
637 Nemitz, E., Delia, A. E., Toohey, D. W., Guenther, A. B., and Nandi, S.: Cloud
638 Activating Properties of Aerosol Observed during CELTIC, *J. Atmos. Sci.*, 64, 441–
639 459, 2007.
- 640 Sun, Y., Wang, Z., Dong, H., Yang, T., Li, J., Pan, X., Chen, P., and Jayne, J. T.:
641 Characterization of summer organic and inorganic aerosols in Beijing, China with
642 an Aerosol Chemical Speciation Monitor, *Atmos. Environ.*, 51, 250–259,
643 doi:10.1016/j.atmosenv.2012.01.013, 2012.
- 644 Takegawa, N., Miyakawa, T., Kawamura, K., and Kondo, Y.: Contribution of selected
645 di-carboxylic and omega-oxocarboxylic acids in ambient aerosol to the m/z 44
646 signal of an aerodyne aerosol mass spectrometer, *Aerosol Sci. Technol.*, 41, 418–
647 437, doi:10.1080/02786820701203215, 2007.
- 648 Twohy, C. H. and Anderson, J. R.: Droplet nuclei in non-precipitating clouds:
649 composition and size matter, *Environ. Res. Lett.*, 3, 045002,
650 doi:10.1088/1748-9326/3/4/045002, 2008.
- 651 VanReken, T. M., Rissman, T. A., Roberts, G. C., Varutbangkul, V., Jonsson, H. H.,
652 Flagan, R. C., and Seinfeld, J. H.: Toward aerosol/cloud condensation nuclei (CCN)
653 closure during CRYSTAL-FACE, *J. Geophys. Res.*, 108, 4633,

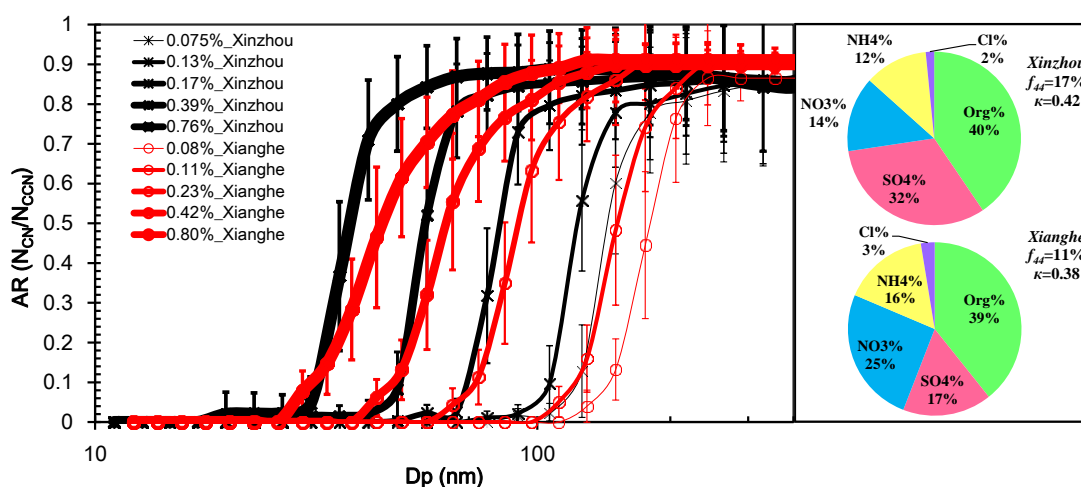
- 654 doi:10.1029/2003JD003582, 2003.
- 655 VanReken, T. M., Ng, N. L., Flagan, R. C., and Seinfeld, J. H.: Cloud condensation
656 nucleus activation properties of biogenic secondary organic aerosol, *J. Geophys.*
657 *Res.*, 110, D07206, doi:10.1029/2004JD005465, 2005.
- 658 Varutbangkul, V., Brechtel, F. J., Bahreini, R., Ng, N. L., Keywood, M. D., Kroll, J.
659 H., Flagan, R. C., Seinfeld, J. H., Lee, A., and Goldstein, A. H.: Hygroscopicity of
660 secondary organic aerosols formed by oxidation of cycloalkenes, monoterpenes,
661 sesquiterpenes, and related compounds, *Atmos. Chem. Phys.*, 6, 2367–2388, 2006.
- 662 Verver, G., F. Raes, D. Vogelezang, and D. Johnson, The 2nd Aerosol characterization
663 Experiment (ACE-2): meteorological and chemical context, *Tellus B*, 2000, 52(2),
664 126-140.
- 665 Wang, J., Lee, Y.-N., Daum, P. H., Jayne, J., and Alexander, M. L.: Effects of aerosol
666 organics on cloud condensation nucleus (CCN) concentration and first indirect
667 aerosol effect, *Atmos. Chem. Phys.*, 8, 6325–6339, doi:10.5194/acp-8-6325-2008,
668 2008.
- 669 Wang, Y.Q., Zhang, X.Y. and Draxler, R., 2009. TrajStat: GIS-based software that
670 uses various trajectory statistical analysis methods to identify potential sources
671 from long-term air pollution measurement data. *Environmental Modelling &*
672 *Software*, 24: 938-939
- 673 Ward, D. S., Eidhammer, T., Cotton, W. R., and Kreidenweis, S. M.: The role of the
674 particle size distribution in assessing aerosol composition effects on simulated
675 droplet activation, *Atmos. Chem. Phys.*, 10, 5435–5447,
676 doi:10.5194/acp-10-5435-2010, 2010.
- 677 Weber, R., P. H. McMurry, R. Mauldin, D. Tanner, F. Eisele, A. Clarke, and V.
678 Kapustin, New particle formation in the remote troposphere: A comparison of

- 679 observations at various sites, *Geophysical Research Letters*, 1999,26(3),
680 307-310.
- 681 Wex, H., Hennig, T., Salma, I., Ocskay, R., Kiselev, A., Henning, S., Massling, A.,
682 Wiedensohler, A., and Stratmann, F.: Hygroscopic growth and measured and
683 modeled critical super-saturations of an atmospheric HULIS sample, *Geophys. Res.*
684 *Lett.*, 34, L02818, doi:10.1029/2006GL028260, 2007.
- 685 Whitby, K., T.: The physical characteristics of sulfur aerosols. *Atmos. Environ.*, 12,
686 135-159, 1967, Online publication date: 1-Jan-1978, 1978.
- 687 Wiedensohler A; Cheng YF; Nowak A; Wehner B; Achtert P; Berghof M; Birmili W;
688 Wu ZJ; Hu M; Zhu T; Takegawa N; Kita K; Kondo Y; Lou SR; Hofeumahaus A;
689 Holland F; Wahner A; Gunthe SS; Rose D; Su H; Pöschl U (2009) Rapid aerosol
690 particle growth and increase of cloud condensation nucleus activity by secondary
691 aerosol formation and condensation: A case study for regional air pollution in
692 northeastern China, *Journal of Geophysical Research: Atmospheres*, 114, . doi:
693 [10.1029/2008JD010884](https://doi.org/10.1029/2008JD010884)
- 694 Yue, D. L., Hu, M., Zhang, R. J., Wu, Z. J., Su, H., Wang, Z. B., Peng, J. F., He, L. Y.,
695 Huang, X. F., Gong, Y. G., and Wiedensohler, A.: Potential contribution of new
696 particle formation to cloud condensation nuclei in Beijing, *Atmos. Environ.*, 45,
697 6070-6077, 2011.
- 698 Zhang, Q., Meng, J., Quan, J., Gao, Y., Zhao, D., Chen, P., and He, H.: Impact of
699 aerosol composition on cloud condensation nuclei activity, *Atmos. Chem. Phys.*, 12,
700 3783-3790, doi:10.5194/acp-12-3783-2012, 2012.
- 701 Zhang, F., Z. Li, R. J. Li, L. Sun, C. Zhao, P. C. Wang, Y. L. Sun, Y. N. Li, X. G. Liu,
702 J. X. Li, P. R. Li, G. Ren, and T. Y. Fan., Aerosol hygroscopicity and cloud
703 condensation nuclei activity during the AC3Exp campaign: implications for cloud

704 condensation nuclei parameterization. Atmos. Chem. Phys., 14, 13423–13437,
 705 2014

706
 707
 708
 709
 710
 711
 712
 713
 714
 715
 716
 717

Figures

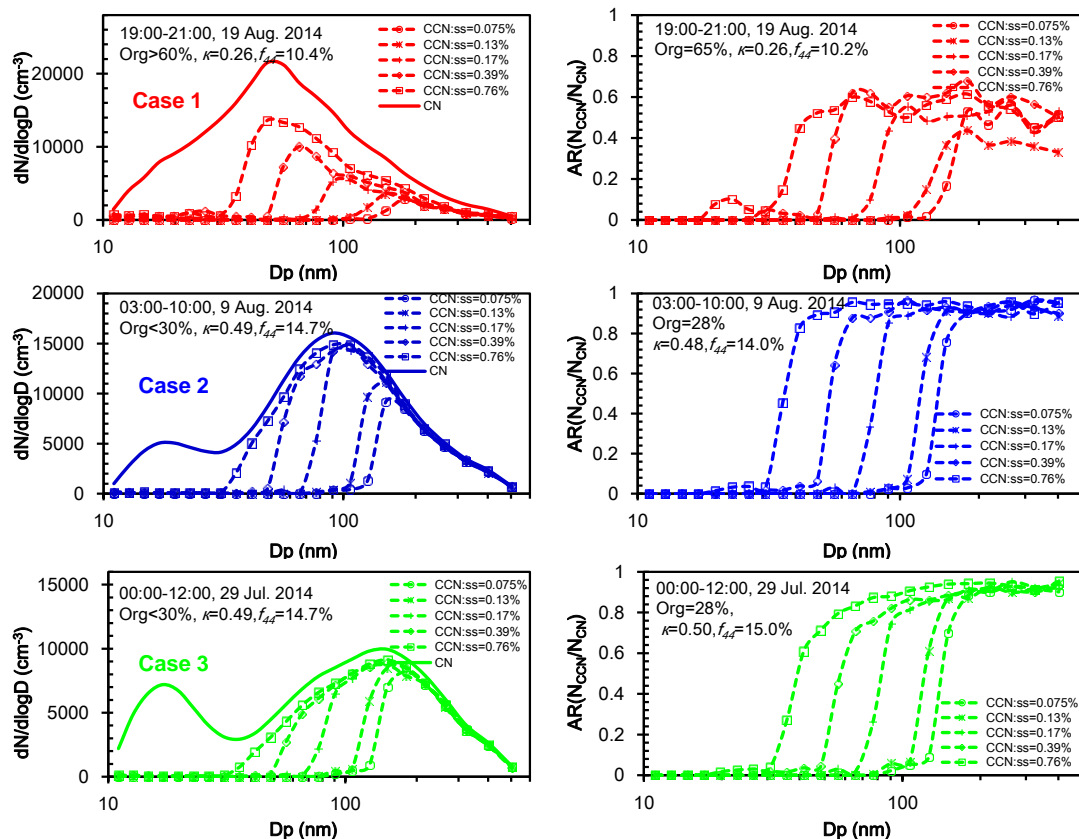


718

719 **Fig. 1.** Mean CCN efficiency spectra at the Xinzhou site (black lines with asterisks)
 720 measured from 22 July–26 August 2014 and at the Xianghe site (red lines with circles)
 721 site measured from 7–21 July 2013 for different supersaturation levels. Error bars
 722 representing one standard deviation are shown. Right panels show particle chemical
 723 composition in terms of mass concentration fractions at Xinzhou (top panel) and
 724 Xianghe (bottom panel) during their respective observation periods. The campaign
 725 average mass concentration of PM_{10} is $31.6 \mu g m^{-3}$ and $72.4 \mu g m^{-3}$ at Xinzhou and
 726 Xianghe respectively. Note that the preset supersaturation levels were 0.07%, 0.1%,

727 0.2%, 0.4% and 0.8% at both sites, but effective supersaturation levels showed
 728 slightly different after calibration.

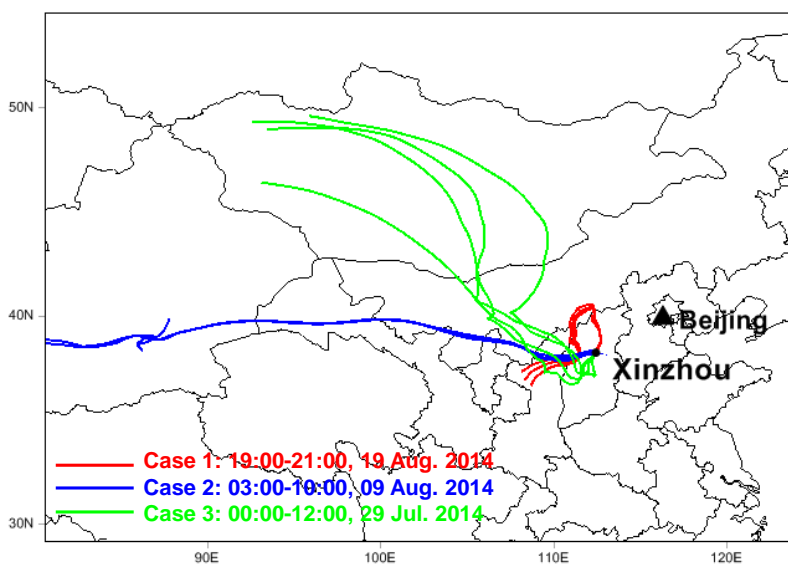
729
 730
 731
 732
 733



734 **Fig. 2.** Particle number size distribution (PSD) and CCN size distributions (left panels)
 735 and CCN efficiency spectra (right panels) at different supersaturation levels for Case 1
 736 (upper panels, 19 August 2014, 19:00-21:00 LT), Case 2 (middle panels, 9 August
 737 2014, 03:00-10:00 LT), and Case 3 (bottom panels, 29 July 2014, 00:00-12:00 LT).
 738 Total CN number concentrations are 16671 cm^{-3} , 12869 cm^{-3} , and 10134 cm^{-3} for
 739 Case 1, Case 2, and Case 3, respectively. Mass concentrations of PM_{10} are $28.36 \mu\text{g}$
 740 m^{-3} , $81.45 \mu\text{g m}^{-3}$, and $78.73 \mu\text{g m}^{-3}$ for Case 1, Case 2 and Case 3, respectively.
 741

742
 743
 744
 745

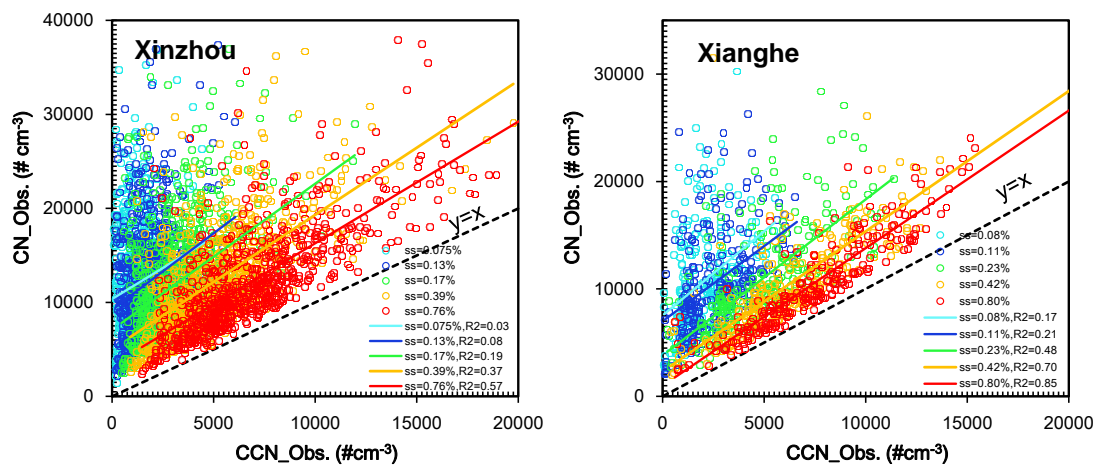
746
747
748
749
750
751



752
753
754
755
756
757
758
759
760
761
762
763
764
765
766
767
768
769

Fig. 3. Five-day back trajectories for Case 1 (in red), Case 2 (in blue), and Case 3 (in green) calculated using the Hybrid Single-Particle Lagrangian Integrated Trajectory model with National Centers for Environmental Prediction reanalysis data. The arrival height of the trajectories at the Xinzhou site was at the surface.

770
771
772
773
774
775

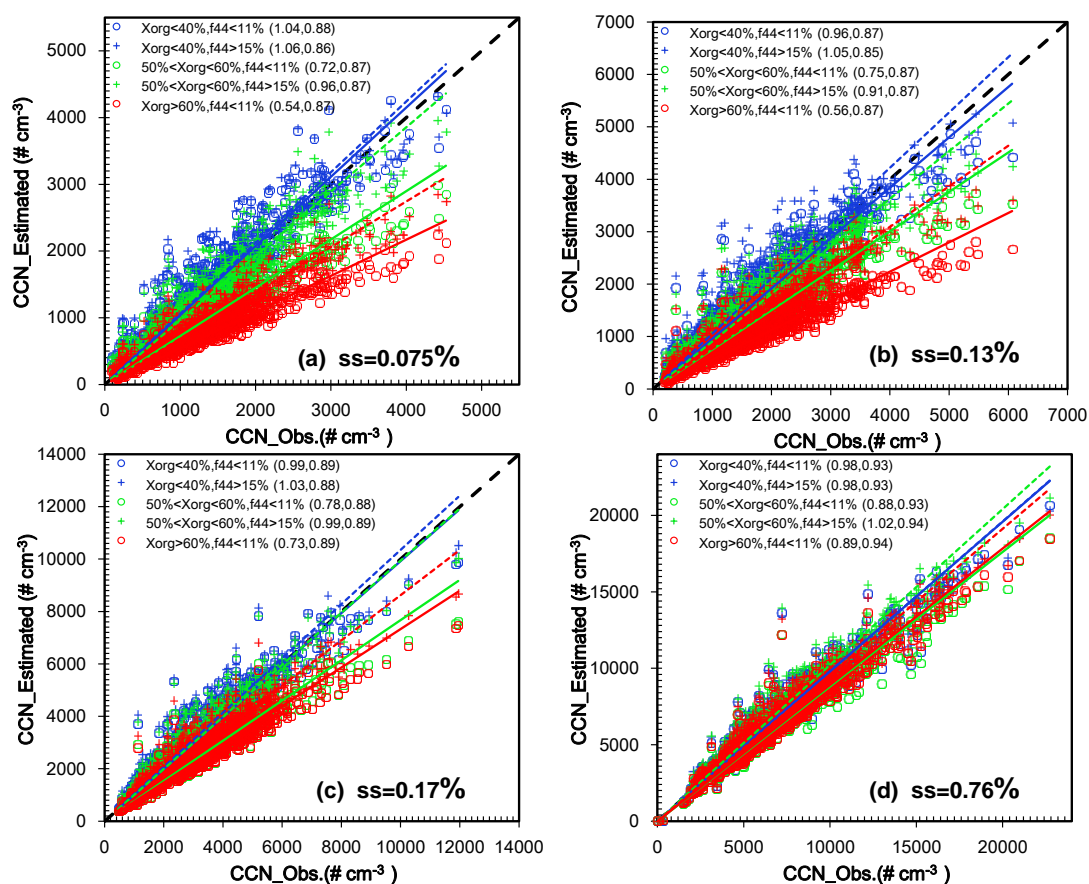


776
777
778
779
780
781

Fig. 4. Measured N_{CN} as a function of measured N_{CCN} for different supersaturation levels at the Xinzhou (left panel) and Xianghe (right panel) sites. The scatterplot between CCN_{Obs} and CN_{Obs} were fitted with a linear function (in colored lines) and R^2 refer to the correlations of them.

782
783
784
785
786
787
788
789
790
791
792
793
794
795
796

797
798
799
800
801
802



803

804 **Fig. 5.** The sensitivity of N_{CCN} to both organics volume fraction (x_{org}) and oxidation
805 level (using f_{44} , the fraction of m/z 44 in aerosol organic material) of organics at
806 supersaturation levels of (a) 0.075%, (b) 0.13%, (c) 0.17% and (d) 0.76% for cases
807 when $x_{org} = 35\%$ (blue circles), 52% (green circles), and 66% (red circles). The
808 size-resolved CCN data were sorted when the $x_{org} > 60\%$, $50\% < x_{org} < 60\%$ and $x_{org} < 40\%$
809 respectively to do the sensitivity examination. Linear best-fit lines through each group of
810 points are shown. Slopes and R^2 values are given in parentheses.

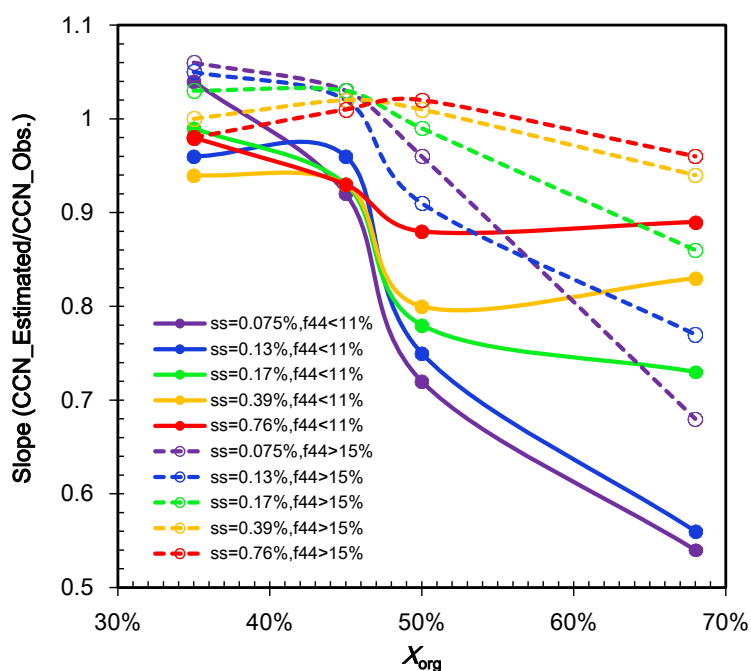
811

812

813

814

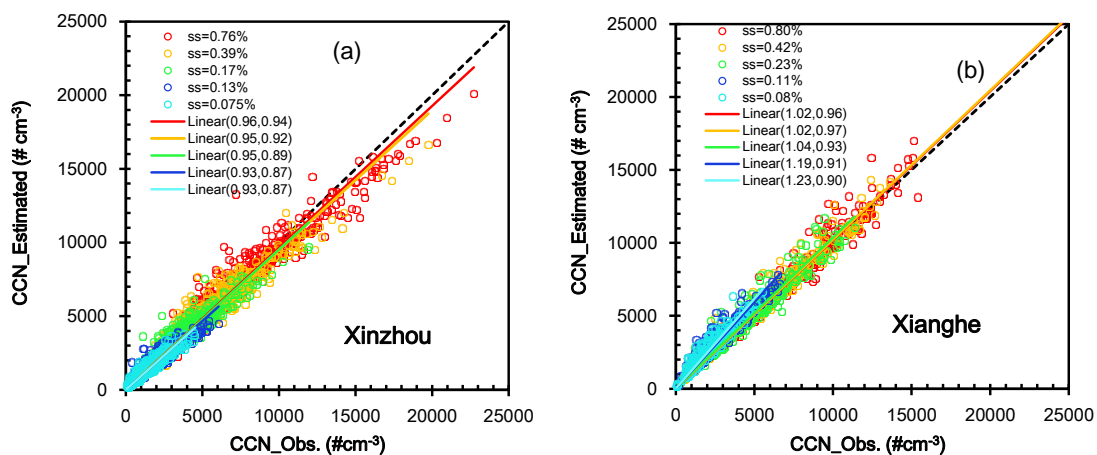
815
816
817
818
819
820
821
822



823
824
825
826
827
828
829
830
831
832
833
834
835
836

Fig. 6. Slopes of the linear fit of estimated and observed N_{CCN} dependence on volume fraction of organics (x_{org}) at $f_{44} < 11\%$ and $f_{44} > 15\%$ for different supersaturation levels. Mean values of the hygroscopic parameter κ_{chem} at $f_{44} < 11\%$ when $x_{org} > 60\%$, $50\% < x_{org} < 60\%$, $40\% < x_{org} < 50\%$ and $x_{org} < 40\%$ are 0.27, 0.34, 0.40 and 0.46, respectively; while at $f_{44} > 15\%$ the value increased to 0.36, 0.42, 0.46 and 0.50 respectively.

837
838
839
840
841
842
843
844



845
846
847
848
849
850
851
852
853
854
855
856
857
858

Fig. 7. Estimated N_{CCN} as a function of observed N_{CCN} for different supersaturation levels at (a) Xinzhou and (b) Xianghe. Note that the campaign mean CCN efficiency spectra at Xinzhou are used for estimating N_{CCN} at Xianghe. Linear best-fit lines through each group of points are shown. Slopes and R^2 values are given in parentheses.